Nightside auroral zone and polar cap ion outflow as a function of substorm size and phase

G. R. Wilson and D. M. Ober
Mission Research Corporation, Nashua, New Hampshire, USA

G. A. Germany
Center for Space Plasma and Aeronomic Research, University of Alabama in Huntsville, Huntsville, Alabama, USA

E. J. Lund
Space Science Center, University of New Hampshire, Durham, New Hampshire, USA

Received 8 January 2003; revised 29 October 2003; accepted 13 November 2003; published 13 February 2004.

[1] Because the high latitude ionosphere is an important source of plasma for the magnetosphere under active conditions, we have undertaken a study of the way ion outflow from the nightside auroral zone and polar cap respond to substorm activity. We have combined data from the Ultraviolet Imager (UVI) on Polar with ion upflow measurements from the TEAMS instrument on the FAST spacecraft to construct a picture of ion upflow from these regions as a function of substorm size and as a function of time relative to substorm onset. We use data taken during solar minimum in the northern hemisphere between December 1996 and February 1997. We find that the total nightside auroral zone ion outflow rate (averaged over substorm phase) depends on the size of the substorm, increasing by about a factor of 10 for both O^+ and H^+ from the smallest to the largest substorms in our study. The combined outflow rate from both the polar cap and the nightside auroral zone goes up by a factor of 7 for both ions for the same change in conditions. Regardless of storm size, the nightside auroral zone outflow rate increases by about a factor of 2 after onset, reaching its peak level after about 20 min. These results indicate that the change in the nightside auroral zone ion outflow rate that accompanies substorm onset is not as significant as the change from low to high magnetic activity. As a consequence, the prompt increase in the near earth plasma sheet energy density of O^+ and H^+ ions that accompanies onset [*Daglis and Axford*, 1996] is likely due to local energization of ions already present rather than to the sudden arrival and energization of fresh ionospheric plasma. *INDEX TERMS:* 2788 Magnetospheric Physics: Storms and substorms; 2704 Magnetospheric Physics: Auroral phenomena (2407); 2736 Magnetospheric Physics: Magnetosphere/ionosphere interactions; 2776 Magnetospheric Physics: Polar cap phenomena; 2407 Ionosphere: Auroral ionosphere (2704); *KEYWORDS:* ion outflow, substorm phenomena, auroral zone, polar cap, magnetosphere-ionosphere interaction

Citation: Wilson, G. R., D. M. Ober, G. A. Germany, and E. J. Lund (2004), Nightside auroral zone and polar cap ion outflow as a function of substorm size and phase, *J. Geophys. Res.*, *109*, A02206, doi:10.1029/2003JA009835.

1. Introduction

[2] In this paper we will focus on what we call suprathermal outflow, that is, ions with energies well above typical ionospheric values ($\geq$10 eV). At energies above 10 eV all ions, including the heavier ones, have the ability to escape from the Earth from the altitude at which they are observed. These ions have undergone energization, very likely by some type of wave process [*Norqvist et al.*, 1998], before their observation. They are closely associated with high latitude regions where energy dissipation occurs (i.e., the auroral zone and the cusp). Ion outflows have been the subject of extensive study by numerous instruments carried on many polar orbiting satellites (S3-3, Akebono, DE-1, Viking, Freja, FAST, Polar, etc.) (see reviews by *André and Yau* [1997] and *Yau and André* [1997]).

[3] Large satellite databases have been used to perform statistical studies of energized ion outflow to find the average outflows as a function of position, season, solar activity and magnetic activity. A significant contribution to this effort was made by A. Yau in a series of papers published in the mid-1980s and whose results are summarized by *Yau et al.* [1998]. Much of the DE1/EICS data used by *Yau et al.* [1998] was reanalyzed by *Collin et al.* [1989]. The conclusion of their work is that the total outflow rates for H^+, He^+, and O^+ (i.e., number of ions per second leaving the high-latitude ionosphere) increase by factors of 4, 5.7,

0148-0227/04/2003JA009835$09.00

and 25, respectively, for an increase of Kp from 0 to 6. An increase in solar EUV (as indicated by an increase in $F_{10.7}$ from 70 to 300 $\times$ 10^{-22} W m^{-2} Hz^{-1}) does not result in a significant change in the H^+ outflow rate but increases the He^+ rate by a factor of 16 and the O^+ rate by a factor of 20. *Peterson et al.* [2001], using data from the Polar/TIMAS instrument, show how outflow rates vary with season. In particular, they see a factor of 2.6 increase in the He^+ outflow rate from summer to winter.

[4] Although it has been demonstrated that suprathermal ion upflow is statistically associated with the auroral oval, how well does the correlation hold up in a near instantaneous comparison? *Stevenson et al.* [2001] show several examples of Polar perigee pass data from the Thermal Ion Dynamics Experiment (TIDE) and the Ultraviolet Imager (UVI) which show a close correlation between auroral forms and large upward O^+ parallel velocities (10–20 km/s). In particular, one can see an abrupt change from downward to upward O^+ flow just at the point where Polar crosses the high-latitude boundary of the nightside auroral oval in the cases shown in that paper. *Tung et al.* [2001] describe ion conic outflow observed by the FAST spacecraft on the poleward side of the aurora near midnight. They note that the probability of observing one of these large upflow events depends on how active the aurora is in the region where the FAST crossing occurs and that this probability increases with increasing time after substorm onset. However, these events can be observed any time the aurora is active, regardless of whether or not a nearby onset can be identified. In our work with some of the same data [*Wilson et al.*, 2001] we note a strong correlation between large O^+ upflow fluxes observed by FAST and the intensity of the aurora at the foot point of the field line on which the fluxes were observed. For an increase from 0 to 4 kR in the LBH-l band (1600–1800 Å) emissions, the O^+ outflow flux can increase by a factor of 100 [*Wilson et al.*, 2001].

[5] Because of the close correlation of nightside upflows with nightside auroral activity it is natural to suspect that this ion outflow will respond on substorm time scales. *Daglis and Axford* [1996] argue for the prompt supply of ionospheric ions to the near earth plasma sheet as a result of substorm onset because of a measured prompt increase in the O^+ plasma sheet pressure at onset. Because this pressure increase is a result of an increase in the energy density of the higher energy particles (17–300 keV) it is not clear how much of it is due to an influx of more ionospheric ions or an influx of external energy to the plasma sheet. In analyzing Geotail data, *Nosé et al.* [2000] note that the energy of both O^+ and H^+ ions in the plasma sheet increase near simultaneously with local depolarization, with the O^+ increase being larger than that for H^+.

[6] *Øieroset et al.* [1999] used Viking ion upflow data between 40 eV and 1.2 keV to characterize the change in dayside ion outflow characteristics as a function of AE or substorm phase. They find that as a substorm cycles from quiet to growth to expansion and then to the recovery phase the average upflowing ion flux across the whole dayside goes from 2.8 $\times$ 10^7 to 4.0 $\times$ 10^7 to 5.8 $\times$ 10^7 and then drops to 3.8 $\times$ 10^7 cm^{-2} s^{-1} (fluxes normalized to 1000 km altitude). In the cusp region the increase in the average flux is greater than these numbers indicate (factor of 2.6 versus 2.0) but is offset by smaller increases in the prenoon and postnoon regions. Although the authors of this paper do not give it, it appears from the doubling of the average flux (from quiet to expansion) and the near doubling of the area covered by the dayside auroral zone for the same change, that the total outflow rate from the dayside auroral zone will go up by a factor of 4 between quiet conditions and the expansion phase of a substorm.

[7] Why is ion outflow on substorm time scales important? It is well know that the relative amount of O^+ in the magnetosphere goes up during active times as is evident by changes in the composition of the ring current during the main phase of a magnetic storm [*Young et al.*, 1982; *Kozyra et al.*, 2002]. The ring current is supplied by plasma from the near-Earth plasma sheet, which is itself supplied with plasma from the high-latitude ionosphere and the magnetosheath. The abundance of O^+ in the storm time ring current testifies to the importance of the ionospheric source under active conditions. Multiple substorms often occur during the main phase of a magnetic storm and the question has arisen as to what contribution these substorms make to the plasma supplied to the inner magnetosphere that feeds the ring current. Do they merely act to inject plasma from the tail or do they also act to increase the plasma content of the near earth plasmasheet through enhanced ion outflow. The answer to this question depends on an understanding of how ion outflow responds to substorm activity.

[8] There are several high-latitude regions, which can supply plasma that ultimately gets to the plasma sheet. These are the cleft ion fountain, the polar cap, and the nightside auroral zone. It is generally believed that the cleft ion fountain would be the strongest of these three sources, but the nightside auroral zone has the most direct access to the inner plasma sheet. The outflow from each region will change with the level of activity but the nightside auroral zone should be the most responsive to changing conditions in the magnetotail. To understand which source region is most important for the inner plasma sheet, we need to know in what way and how quickly the various ionospheric source regions respond to magnetic activity. We also need to understand how the ionospheric plasma from the various source regions is transported and energized on its way to the plasma sheet [*Moore and Delcourt*, 1995; *Winglee*, 1998].

[9] In this paper we use FAST/TEAMS data combined with Polar/UVI data to estimate the regional ion outflow rates from the nightside auroral zone and polar cap as a function of substorm phase. The UVI data is used to identify the onset time, to characterize the severity and duration of the substorm, and to determine the sizes of the auroral zone and polar cap as a function of time. The TEAMS data is used to determine average O^+ and H^+ number fluxes as a function of position and time during the substorm. Putting these two together allows us to find the regional ion outflow rates. One side benefit of our study was to determine how the nightside auroral zone and polar cap outflow rates changed with the size of the substorm.

2. Data Description

[10] The data used in this paper comes from two sources. The first is the Time-of-Flight Energy Angle Mass Spectrometer (TEAMS) instrument [*Möbius et al.*, 1998] on the FAST spacecraft and the second is the Ultraviolet Imager

(UVI) [*Torr et al.*, 1995] on Polar. This is the same data that was used in our previous study [*Wilson et al.*, 2001] but has been extended to cover most of the three month winter period of December 1996 to February 1997.

[11] The TEAMS instrument is able to separate ions by arrival angle, energy per charge, and mass per charge. The front end of the instrument is a toroidal top hat type electrostatic analyzer (ESA) with a 360° × 8° field of view. It is mounted on the spacecraft so that it will sweep out a full 4π sr in half of a spacecraft spin. Behind the ESA, ions are accelerated up to maximum of 20 kV and sent through a time-of-flight section for mass discrimination. The instrument has an energy range of 3 eV to 12 keV, can readily identify the major ion species (H^+, He^{++}, He^+, O^+), and has a time resolution of 2.5 s which is half of the spacecraft spin period. (Most of the TEAMS data we used in this study had a 5 s time resolution.) Its angular resolution is 22.5° × 22.5°. We do not process the TEAMS data in any way to remove ram effects or the effects of spacecraft potential. To mitigate these effects, we restrict our attention to ions whose energy exceeds 8 eV, an energy larger than the typical ram energy (≤4 eV) or spacecraft potential energy (3 eV). The TEAMS measurements were turned into field-aligned fluxes of H^+ and O^+ ions by integrating over part of the energy-pitch angle data space. This region excluded the loss cone and extended from 8 eV to 6 keV. Doing this covered most of the suprathermal ion outflow (beams and conics), while suppressing contributions of precipitating ions that could mirror and pose as ion outflow. The resultant fluxes are then mapped to 1000 km altitude.

[12] The Polar Ultraviolet Imager operates in the far ultraviolet (1200–1800 Å) so that it is able to view the sunlit portion of the aurora. It has a circular field of view of 8° with an angular resolution of 0.04°. From apogee this gives a spatial resolution of 30 km. Images are made in four bands centered at 1304, 1356, 1490, and 1700 Å with bandwidths of 50, 70, 175, and 180 Å, respectively. The last two of these filters respond primarily to molecular nitrogen Lyman-Birge-Hopfield (LBH) emissions and are referred to as the LBH-short (LBH-s) and LBH-long (LBH-l) filters. All of the data used in this paper were from images taken with the LBH-l filter. These were flat field corrected and converted into absolute radiance units (kilorayleighs) and had instrument background removed. No effort was made to remove dayglow, which should have little effect on emission intensities from wintertime aurora. During all of the passes used, the UVI was operating in a mode where it would take two exposures with the LBH-s filter (18 and 37 s), followed by two exposures using the LBH-l filter (18 and 37 s, both of which are used), followed by a background reading. The overall timing of the imaging sequence was designed so that the time interval between successive images of the same type was fixed at 3 min 4 s. Because of this, the time spacing between consecutive LBH-l images can be as short as 37 s or as long as 147 s. Passes with significant numbers of missing images were not used. Due to a mass imbalance in the Polar spacecraft that causes it to wobble while it spins, the UVI images are smeared in one direction. We made no effort to correct the images for this effect. The auroral images used in this study were made by averaging images from a minimum of 16 substorms scattered throughout the 3-month study interval. The precession of Polar's orbit plane over this interval assures that the reduced spatial resolution caused by the wobble does not introduce a systematic effect.

[13] Since our concern here is the relationship of ion outflows to substorm activity we first had the task of identifying substorm time intervals during the 3-month interval. We were greatly aided in this by the efforts of K. Liou at The Johns Hopkins University Applied Physics Laboratory who assembled a series of substorm movies made using UVI images [*Liou et al.*, 2001]. From the Liou et al. list of substorms and a few others that we were able to identify, we came up with a list of 127 substorms for which we had UVI images and TEAMS ion outflow measurements. These substorms were also characterized as being isolated in that no two onsets occurred within 2 hours of each other. The substorms are listed in Tables A1 (December 1996), A2 (January 1997), and A3 (February 1997) in Appendix A.

[14] As noted above, the time interval used for this study was restricted to one season and a short portion of a solar cycle. One reason for doing this is to minimize the contribution of other factors (besides substorm activity) that are known to affect ion outflow fluxes. As *Peterson et al.* [2001] and *Yau et al.* [1985] have pointed out, ion outflow fluxes depend on season and solar activity. For our data set, solar minimum conditions apply with the average of the $F_{10.7}$ index being 73 ($\times 10^{-22}$ W m^{-2} Hz^{-1}). During the 3-month interval, $F_{10.7}$ never got higher than 86 or less than 69. Generally speaking, this time interval was magnetically quiet with an average Kp (averaged through Ap) at the time of the substorms of 2+. There was however a great deal of variability in magnetic activity with Kp varying from 0 to 7 at the times of the various substorms. Another reason for choosing a short time interval is to eliminate the effect that changing TEAMS sensitivity would have on the ion measurements.

[15] What we have then is a set of ion upflow measurements made in the nightside auroral zone or polar cap during the growth, onset, expansion or recovery phases of 127 substorms. The upflow measurements are not dense enough to fully populate the three dimensional space of MLT (Magnetic Local Time), MLat (Magnetic Latitude (at 1000 km altitude)), and time so we have combined them to get reduced quantities such as the regional ion outflow rate for the nightside auroral zone, or the polar cap, as a function of time. This process of analysis involves averaging the data and could be done in a number of different ways. The next section will describe two such ways.

3. Results

[16] In this work we combine data about the aurora from TEAMS and UVI to determine the change in ion outflow as a function of substorm phase. Because the TEAMS data is not sufficiently dense in space and time to entirely do the job on its own we will rely on the UVI data set to do such things as define the time of onset and duration of the substorm, to determine when a TEAMS flux measurement is made over the auroral zone, and to give the areas of the auroral zone and polar cap as functions of time. An important question to answer then is how to divide up the TEAMS data so that average fluxes can be found at different points in space and time during the course of a

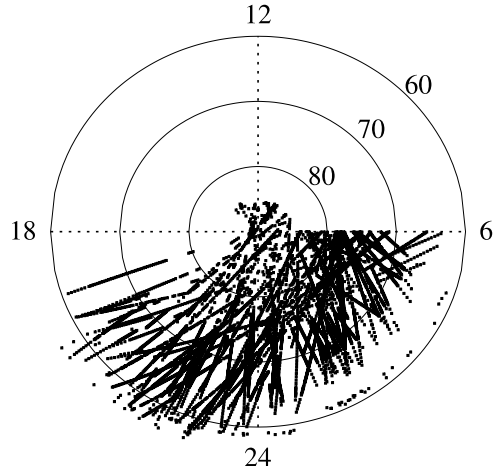

Figure 1. Locations of the FAST spacecraft in MLT-MLat space where TEAMS measurements were made that are used in this study. The spacecrafts position was mapped from altitude down to 100 km along an IGRF magnetic field line.

substorm. The TEAMS data can be sorted by substorm size, substorm phase (time), and location. It would be easy, however, to create so many sort bins that the number of data points per bin was too small to yield meaningful averages. The other extreme would be to ignore all variations in substorm size, location, and time and simply average all of the TEAMS data together. (The average O^+ and H^+ fluxes for all the TEAMS data used in this paper are 2.3×10^6 and 3.7×10^6 cm^{-2} s^{-1}, respectively.) The polar cap and nightside auroral zone outflow rates for this simplest of all approaches are then determine by multiplying the areas of these regions by these average fluxes. More sophisticated approaches will divide the TEAMS data up into smaller groups for averaging but taking care not to carry this dividing process too far that we end up with statistically meaningless averages.

3.1. First Approach

[17] To begin we take 10646 TEAMS O^+ and H^+ ion flux measurements that were made within a 2-hour interval that extended from 30 min before onset to 90 min after onset for substorms in our list. The location of FAST (projected along the magnetic field to 100 km altitude) when the measurements were made is shown plotted versus MLT and MLat in Figure 1. As can be seen, the data selected is from the nightside between the north magnetic pole and about 60° MLat. Dayside measurements were restricted to latitudes above 85° so as to minimize the contribution from ion upflows that originate in the dayside auroral zone or cleft ion fountain. For each of the FAST passes there exists a series of UVI images so that each TEAMS measurement could be associated with the intensity of the aurora at that location. This is done by taking the UVI image that is closest in time (at a time before the TEAMS measurement) and averaging the value of the image pixels that are within 1° of the FAST foot point. This averaging was done to reduce noise in the UVI data such as fluctuations around a luminosity of zero kR in the polar cap. If no image was within two minutes of the TEAMS measurement time, or if the FAST foot point fell outside the FOV of the UVI image the data point was not used.

[18] Figure 2 illustrates how we have divided up the TEAMS data to find average ion fluxes for this approach. The basic approach here is to sort the ion flux measurements by the intensity of the aurora at the foot point of the field line, along the lines of what was done in our previous study [*Wilson et al.*, 2001]. When the luminosity exceeds 0.1 kR this approach can readily identify points that are in the auroral zone. When the foot point luminosity is less than 0.1 kR the point in question may be over the auroral zone (when the flux of precipitating electrons above 2 keV is low), the polar cap or at subauroral latitudes. Not surprisingly, there is a large spread in the range of ion fluxes for these low luminosity cases. The plots of average ion flux versus magnetic latitude shown in Figure 2b for O^+ ions and in Figure 2d for H^+ ions show that low luminosity ion fluxes peak in the auroral zone and are lowest in the middle of the polar cap. To further refine our approach then we divide the low luminosity ion fluxes up into two bins, one for the auroral zone (60°–75°) and one for the polar cap (75°–90°).

[19] Figures 2a and 2c show the average O^+ and H^+ ion flux versus auroral luminosity. The data points used for the two values below 0.1 kR were restricted to the 60°–75° magnetic latitude range. The curve defined by these nine averages determines our relationship between auroral luminosity and ion flux. We have fit the following equation:

$$\mathrm{Log}_{10} F(O^+, H^+) = a(1 - \exp(-bL^c)) + d \qquad (1)$$

to these points. The value for a, b, c and d for O^+ and H^+ ions are shown in Table 1. The end result of all this is to divide the 10646 TEAMS flux measurements into 10 bins: nine for the auroral zone at different luminosity levels and one for the polar cap (magnetic latitudes greater than 75°). The polar cap O^+ and H^+ average fluxes are 4.0×10^5 and 3.6×10^5 cm^{-2} s^{-1}, respectively.

[20] The difference in behavior between the O^+ curve in Figure 2a and the H^+ curve in Figure 2c may be due to the fact that unheated O^+ ions are gravitationally bound while unheated H^+ ions are not. The flux of H^+ ions that reach the spacecraft with energies above 8 eV then depends only on how effective the heating process is which, presumably, becomes more efficient as the auroral luminosity increases. When heating is most efficient, the H^+ flux above 8 eV will be limited by the H^+ flux reaching the bottom of the heating region which, in turn, is dictated by the ionospheric H^+ limiting flux for the given conditions. For O^+ an increase in the heating rate translates into a larger fraction of heated ions reaching the spacecraft as well as an increase in the flux of ions that reach the heating zone. If, as the heating rate increases it also reaches deeper into the atmosphere, the O^+ flux will continue to increase after the H^+ flux has saturated.

[21] Remember that what is plotted in Figure 2 is the flux of ions with energies above 8 eV. We assume here that increasing auroral luminosity means an increase in the energy available to heat ions. As this energy increases the fraction of escaping H^+ flux that gets energized to >8 eV, while crossing the heating region below the spacecraft, goes up until all of the ions are heated. The flux in Figure 2c is then limited by the average H^+ limiting flux for the nightside high latitude ionosphere under solar minimum winter conditions.

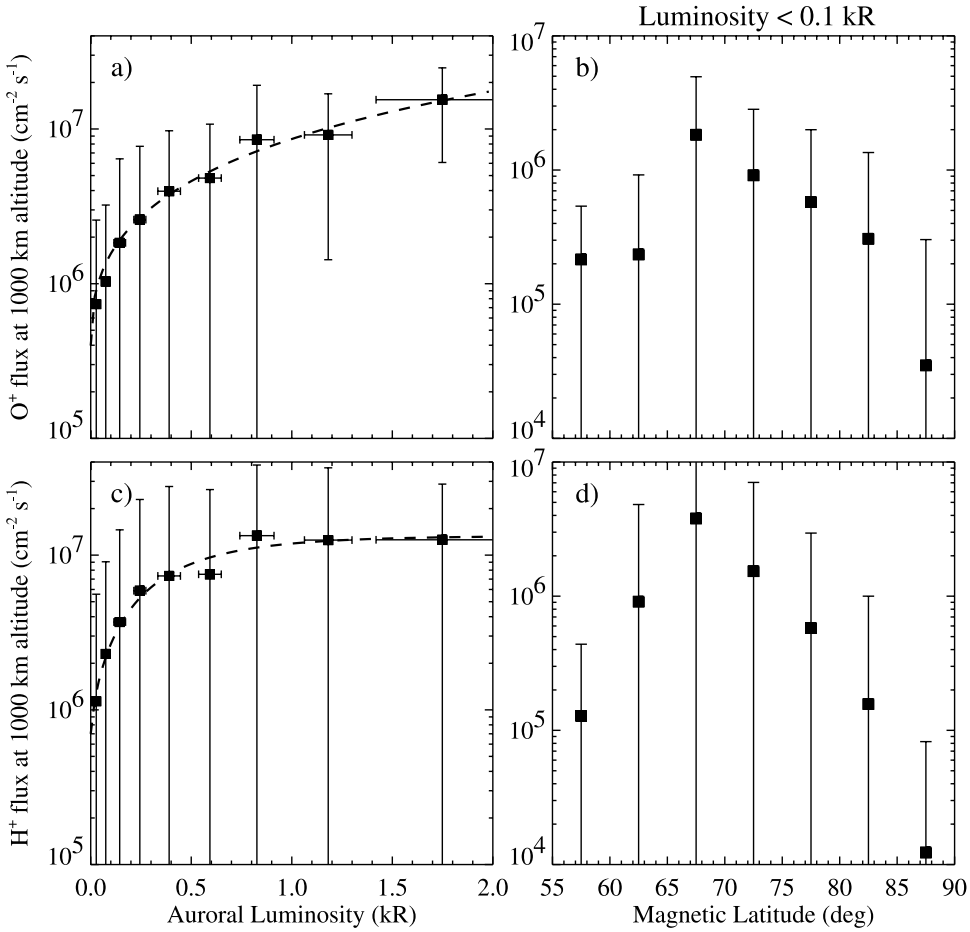

Figure 2. (a) Plot of the average O^+ flux (mapped to 1000 km altitude) as a function of the LBH-l luminosity at the foot point of the field line on which the measurement was made. Data for luminosities below 0.1 kR were restricted to the 60°–75° MLat range. The curve fit to the average values is described in the text. (b) Average O^+ (mapped to 1000 km altitude) plotted versus MLat for data whose foot point luminosity was less than 0.1 kR. (c) Same as Figure 2a but for H^+ ions. (d) Same as Figure 2b but for H^+ ions.

[22] We point out that the "error" bars in Figure 2 indicate the one sigma spread in the values of auroral luminosity and ion flux that were used in the averages. They do not represent the error in the averages. The error in the averages were found by repeatedly calculating the average for each of the 10 bins using randomly selected subsets that consisted of half of the points in each bin. The one sigma spread in the range of these averages was about 10% of the average for each bin. What this means is that the fitted equation (1) gives the average O^+ or H^+ flux versus auroral luminosity to within about 10%.

[23] The curves from Figures 2a and 2c show that there is about a factor of 40(10) increase in the average $O^+(H^+)$ ion flux for an increase of the LBH-l auroral luminosity from 0 to 2 kR. This can be compared with our earlier results [*Wilson et al.*, 2001] for just O^+ where we saw a factor of about 200 increase in the flux for a similar change in luminosity. Part of the reason for this difference is that our earlier results consisted mainly of data from the premidnight sector while this data set includes many points from the dawn sector. Also the previous study did not subdivide the low luminosity points by magnetic latitude. The final reason is that the fitting done in the work of *Wilson et al.* [2001] was done in log space rather than liner space which tends to exaggerate variations if there is a large spread in the value of the quantity being averaged. The results presented here supersede the previous results.

[24] With the results of Figure 2 we can assign a flux to each portion of the nightside and polar cap ionosphere based on its luminosity in the LBH-l band. After carefully examining the substorm movies we grouped the 127 substorms in our list into one of five categories based on their apparent size and duration (small-18, small-medium-22, medium-53, medium-large-18, and large-16). Admittedly, this is a subjective exercise but we crosschecked our list several times making sure that all substorms grouped together really looked similar. We then took the small substorms, grouped their UVI images into 3-min bins, and then produced composite images that averaged the images from the individual substorms together. Because of the

Table 1. Fit Parameters for Equation (1)

	a	*b*	*c*	*d*
H^+	1.3	3.2	0.73	5.8
O^+	3.2	0.54	0.42	5.6

spacing between images each substorm contributed on average two images to each time bin. With 18 small substorms, that is an average of 36 images per time bin. Because of UVI's 8° field-of-view, individual images typically do not cover the whole high-latitude region and sometimes miss parts of the auroral zone. For the small substorms the average number of image pixels per composite image pixel was 29. On the nightside of the composite images that average was 37 owing to the tendency of UVI to concentrate on the nightside region. Also, the spatial extent of the composite image pixels was somewhat larger than the individual substorm image pixels, so some spatial averaging occurred.

[25] Figure 3 shows the 40 small substorm composite images that cover the time interval from 30 min before onset to 90 min after onset. The numbers above each image indicate the averaging time interval relative to onset. As can be seen, the auroral zone is very quiet before onset, and after onset only a small activation region develops slightly premidnight. The aurora returns to relatively quiet conditions within about 50 min. This same type of averaging exercise was repeated for the medium size substorms (53) and large substorms (16). Figures 4 and 5show the 40 composite auroral images for each of these two substorm groups. (In order to conserve space we do not show the corresponding images for the small-medium and medium-large substorm groups since they are what one would expect to see falling between the groups shown.) As can be seen, the intensity of the nightside aurora increases from small to large substorms and the length of the substorms increases with size as well. Also note that the level of activity in the auroral zone before onset is a function of the size of the substorm so that during the growth phase of the average large substorm the nightside aurora is more active than it is at any point during the average small substorm. Incidentally, the average number of image pixels per composite image pixel for the medium substorms was 89 and for the large substorms it was 25. The nightside averages were 120 and 31, respectively.

[26] With the flux versus luminosity relationships from Figure 2 and the auroral substorm information from Figures 3 to 5 it is possible to find the regional nightside auroral zone and polar cap ion outflow rates. This is done by multiplying the area of each pixel, mapped to a spherical surface, by its average ion outflow flux and summing the product over all pixels. The outflow flux is found using the relationships from Figure 2 and the luminosity of each pixel. Pixels on the nightside whose auroral luminosity exceeds 0.1 kR are combined to find the nightside auroral zone outflow rate. Pixels whose luminosity is less than 0.1 kR and are above 70° on the nightside or 78°, 75°, or 73° (small, medium, and large substorms) on the dayside are added up to give the polar cap ion outflow rate. These latitude boundaries are chosen so as to exclude subauroral pixels from the polar cap sum. Also, we assume that the average polar cap ion fluxes found above apply to the whole region identified as polar cap by the UVI images even though the UVI polar cap boundaries may differ from those used in the ion flux averaging. Figure 6 shows these rates as a function of time from substorm onset for the three classes of substorms (small - dashed line; medium - dotted line; large - solid line) for O^+ and H^+ outflow.

[27] From Figure 6 we note that the regional outflow rate from the nightside auroral zone during the growth phase depends on the size of the substorm. For small substorms the growth phase nightside auroral zone outflow rate is comparable to the polar cap outflow rate for O^+ but twice as large for H^+. For large substorms the nightside auroral zone during growth phase produces about 20–30 times as much outflow as the polar cap. After onset the nightside auroral zone outflow rate increases by about a factor of 1.5 to 2 (regardless of substorm size) over a time interval of about 20 min. Note that in the nightside auroral zone the H^+ outflow rates are always higher than the O^+ rates by about a factor of 1.5. Outflow rates from the polar cap either remain constant over the course of the substorm (small, medium) or they decreases during large substorms due to the reduction of the area of the polar cap.

[28] The quantities plotted in Figure 6 are found by summing over the outflow fluxes from individual pixels in the images from Figures 3–5. Each of these individual outflow rates has an error associated with it due to error in the luminosity of the pixel, error in the average flux at that luminosity, and error in the area of the pixel. The UVI sensitivity in the LBH-l filter is 0.1 counts/Integration-Period/R/pixel [*Torr et al.*, 1995]. This gives a signal to noise ratio of 3 and 14 at 0.1 and 2 kR, respectively. For a pixel with a luminosity near 0.1 kR this translates (via equation (1)) into an uncertainty in the O^+ (H^+) flux of about 17% (23%). At 2 kR the uncertainty in O^+ (H^+) flux is about 2% (0.1%). However, because of the uncertainty in the value of the average ion fluxes in Figure 2 there is a minimum in the uncertainty of the ion flux ascribed to each pixel of 10%. The uncertainty in the area is very small since it is a straight geometric calculation on a defined grid. The total error for the nightside auroral zone outflow rate or the polar cap outflow rate is the sum of hundreds or thousands of individual random errors that are at most about 30%. We believe that the overall error should not exceed this value and is likely much less.

3.2. Second Approach

[29] In view of the fact that the above analysis represents an approximation to the true outflow rates, it is instructive to try and get at the same type of answers shown in Figure 6 using a different approach. In place of relating average ion outflow fluxes to auroral luminosities, we bin the outflow data so that we can find the average ion fluxes for O^+ and H^+ for different time intervals during the substorms. Because of our limited TEAMS data we divided the substorms into two groups (small, group 1 and large, group 2) instead of the five groups described above. We do this so that we will have sufficient TEAMS data for various time intervals throughout the substorm. The composite images of the substorm for each group are made by averaging the images from sub-

Figure 3. Images from 18 small substorms were averaged together to produce this sequence of 40 composite images spanning the time interval from 30 min before onset to 90 min after. Each composite image covers a three min interval. The inner and outer circles for each image are at 70° and 50° magnetic latitude, respectively. Onset occurs between images 10 and 11.

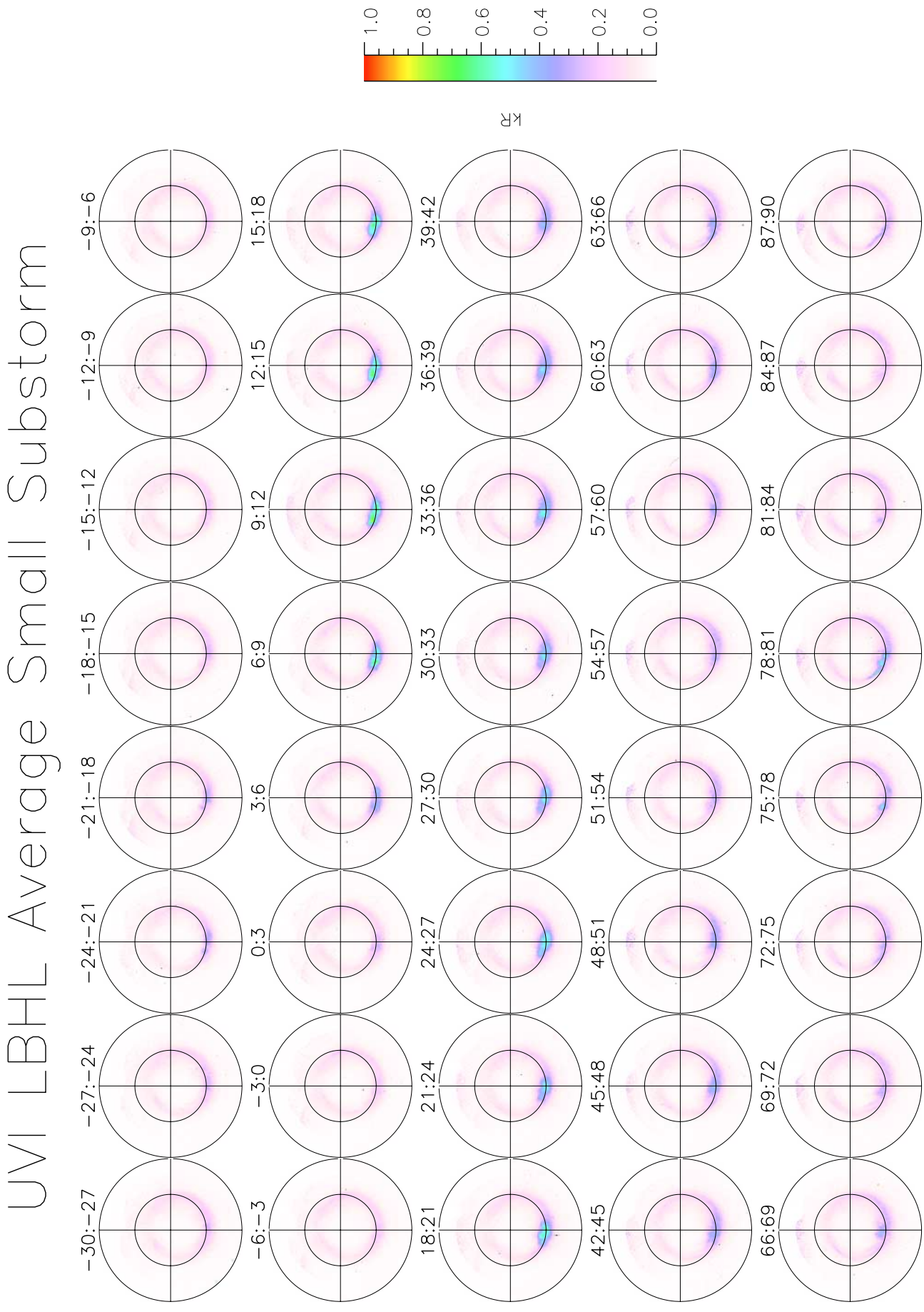
UVI LBHL Average Small Substorm
1.0
0.8
0.6
0.4
0.2
0.0
KR
-30:-27
-27:-24
-24:-21
-21:-18
-18:-15
-15:-12
-12:-9
-9:-6
-6:-3
-3:0
0:3
3:6
6:9
9:12
12:15
15:18
18:21
21:24
24:27
27:30
30:33
33:36
36:39
39:42
42:45
45:48
48:51
51:54
54:57
57:60
60:63
63:66
66:69
69:72
72:75
75:78
78:81
81:84
84:87
87:90

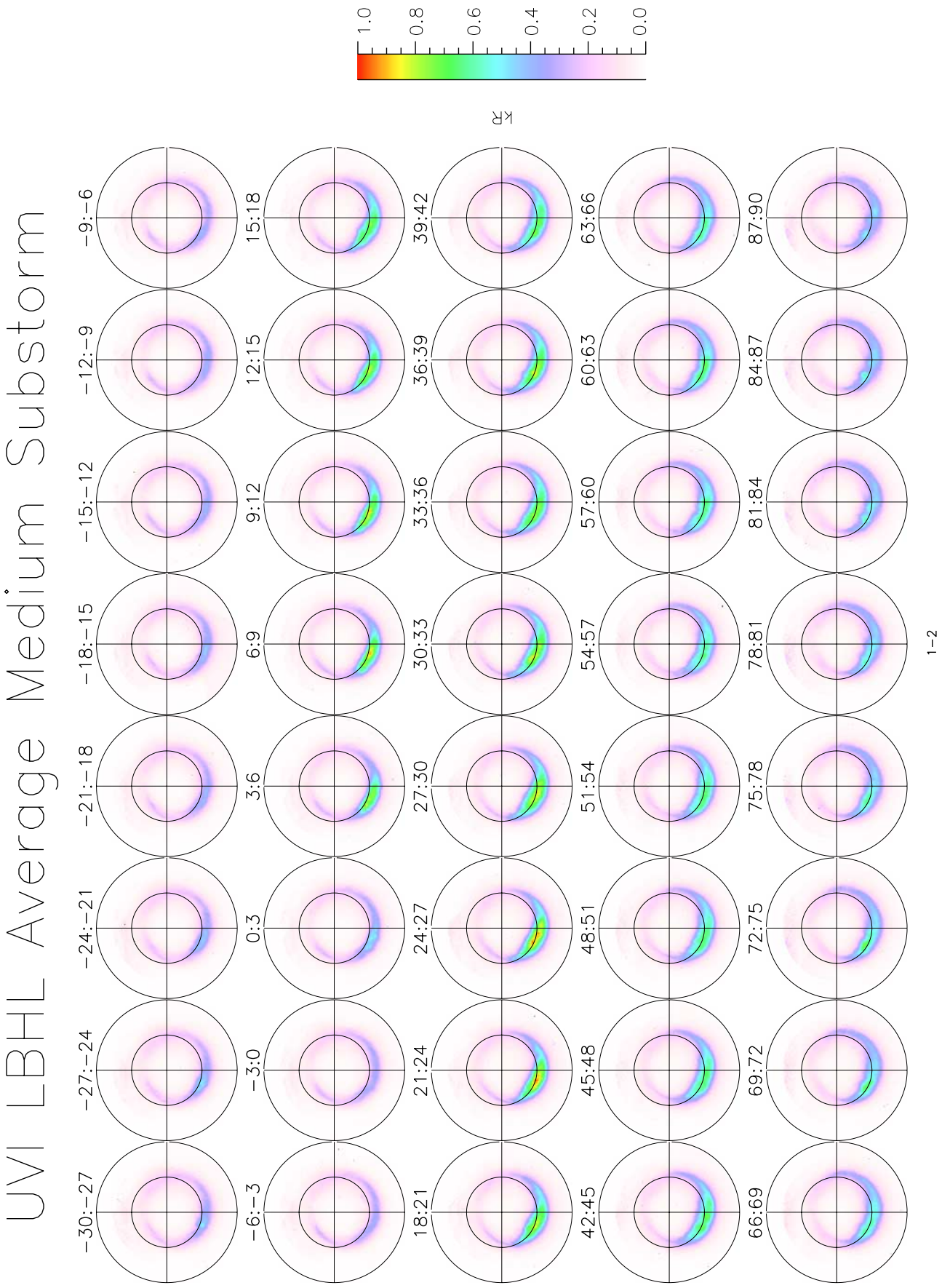

Figure 4. Same as Figure 3 but an average of 53 medium substorms.

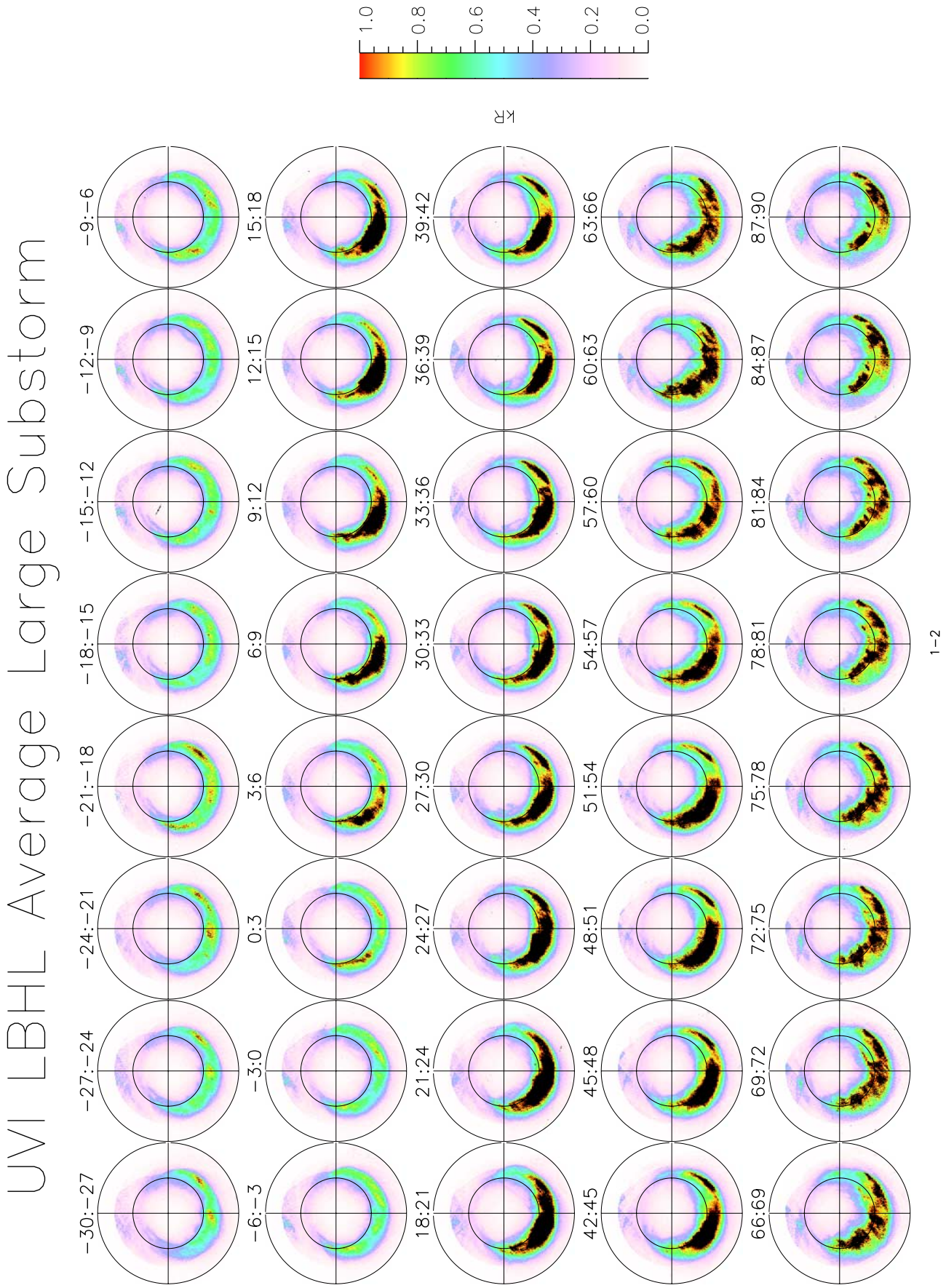

Figure 5. Same as Figure 3 but an average of 16 large substorms.

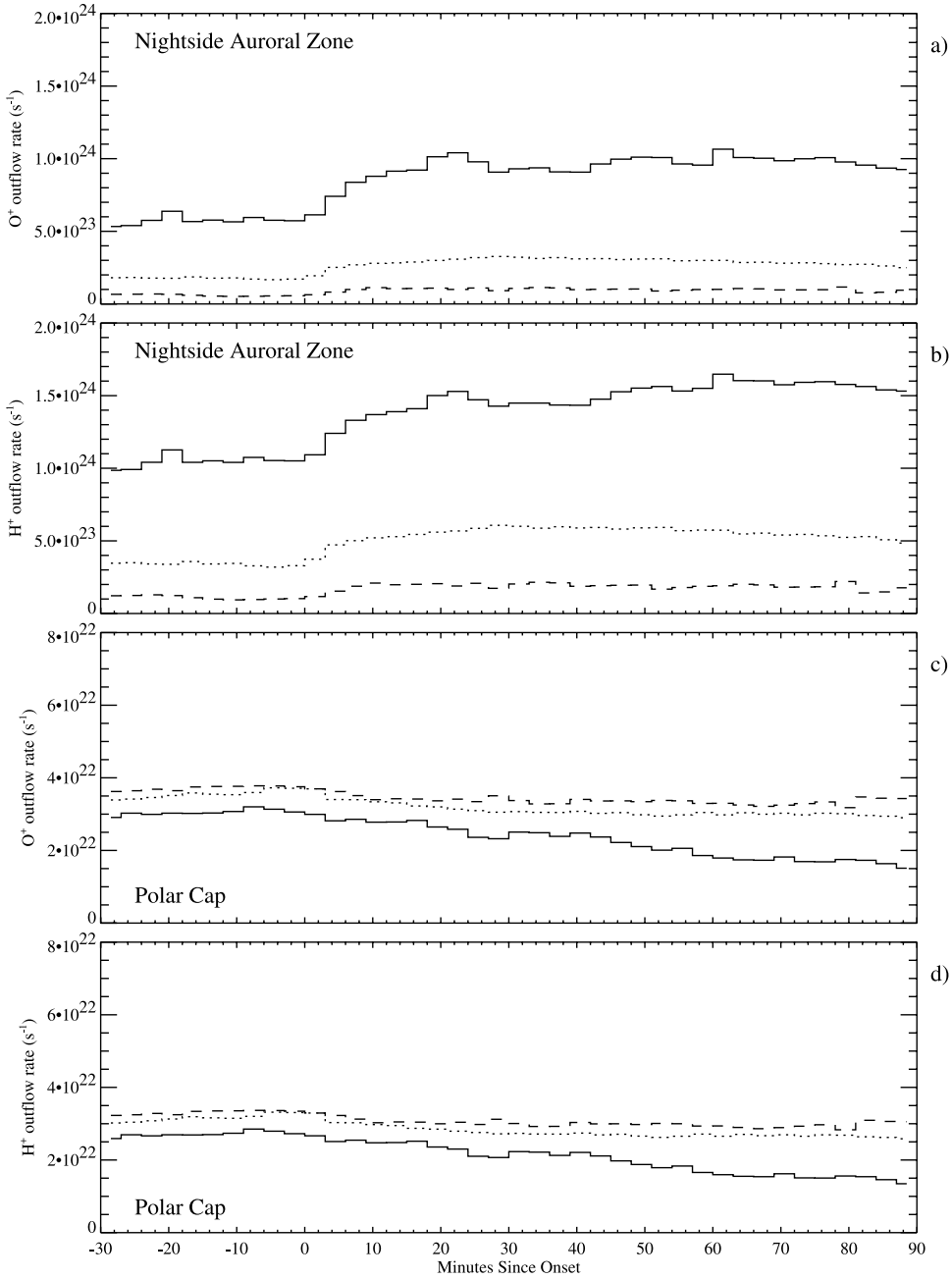

Figure 6. (a) Nightside auroral zone O^+ ion outflow rate as a function of time since onset. Solid line is for large substorms, dotted line is for medium substorms, and dashed line is for small substorms. The nightside auroral zone is defined as any point where MLT $\geq$ 1800 or MLT $\leq$ 0600, MLat $\geq$ 50° and the LBH-l luminosity is $\geq$0.1 kR. (b) Same as Figure 6a but for H^+ ions. (c) Polar cap O^+ ion outflow rate as a function of time since onset. The polar cap is defined as any point poleward of 70° MLat on the night side and 78° (small), 75° (medium), or 73° (large) on the dayside for which the LBH-l luminosity is $\leq$0.1 kR. (d) Same as Figure 6c but for H^+ ions.

storms in the two groups. The dividing line between these two groups is somewhat fuzzy and it falls in the middle of our previous group of medium size substorms. There were 70 group 1 substorms and 57 group 2 substorms. Figures 7 and 8 show what the average small (group 1) and large (group 2) substorm looks like. These images where made in the same way as those shown in Figures 3–5. With these images the area of the polar cap and nightside auroral zone can be found as a function of time.

[30] What is then needed is the average flux of O^+ and H^+ ions from these two regions as a function of time. The nightside auroral zone was defined as that region where MLT >18 or MLT <6, MLat >50° and the LBH-l luminosity $\geq$0.1 kR. The polar cap was defined, for group 1 substorms as any point poleward of 78° on the dayside and 70° on the nightside for which the luminosity $\leq$0.1 kR. For group 2 substorms the dayside MLat boundary was 73°. To illustrate the type of answer we get for the average fluxes, Table 2

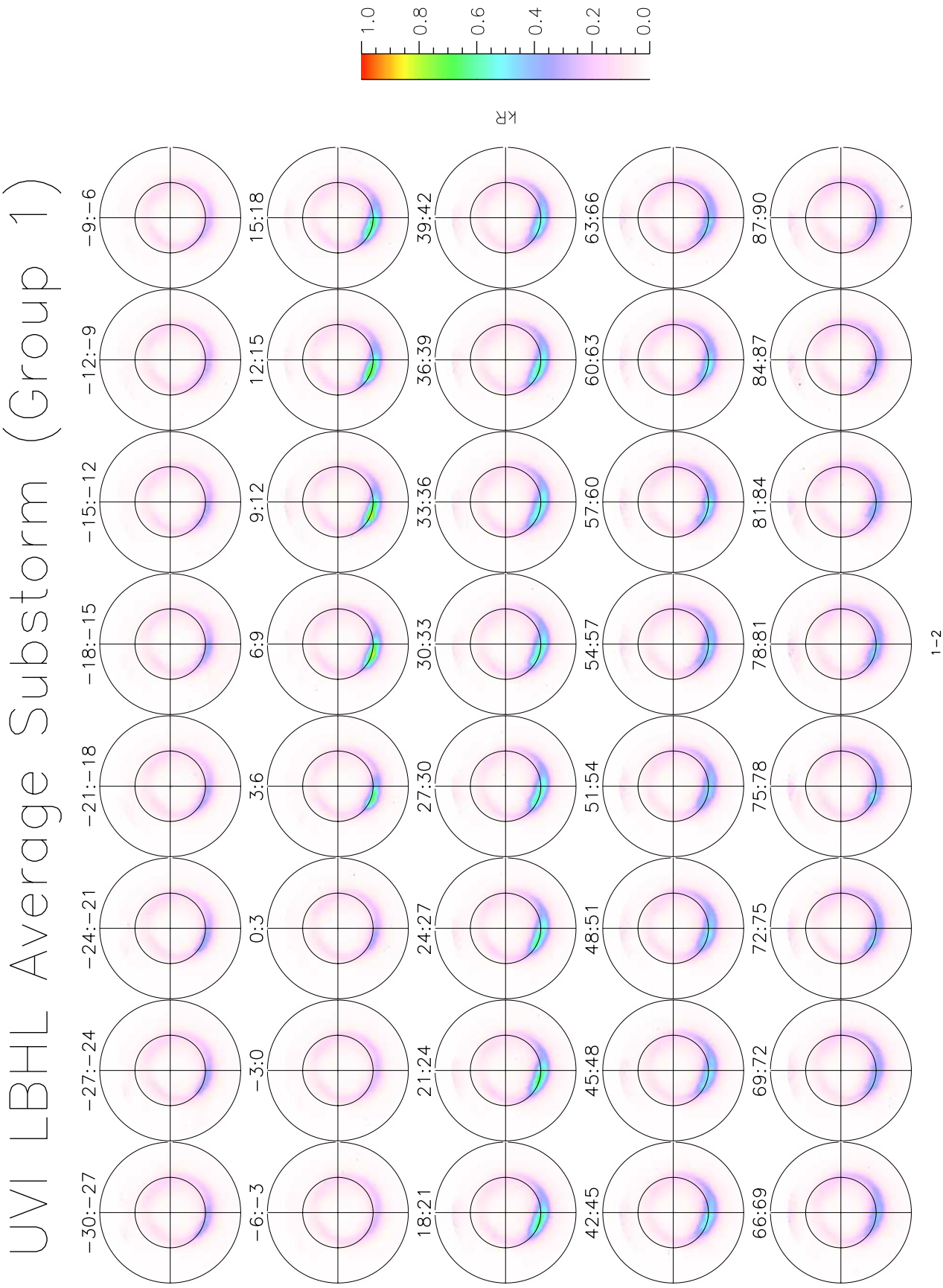

Figure 7. Images from 70 small substorms (group 1) were averaged together to produce this sequence of 40 composite images spanning the time interval from 30 min before onset to 90 min after. Format is the same as Figure 3.

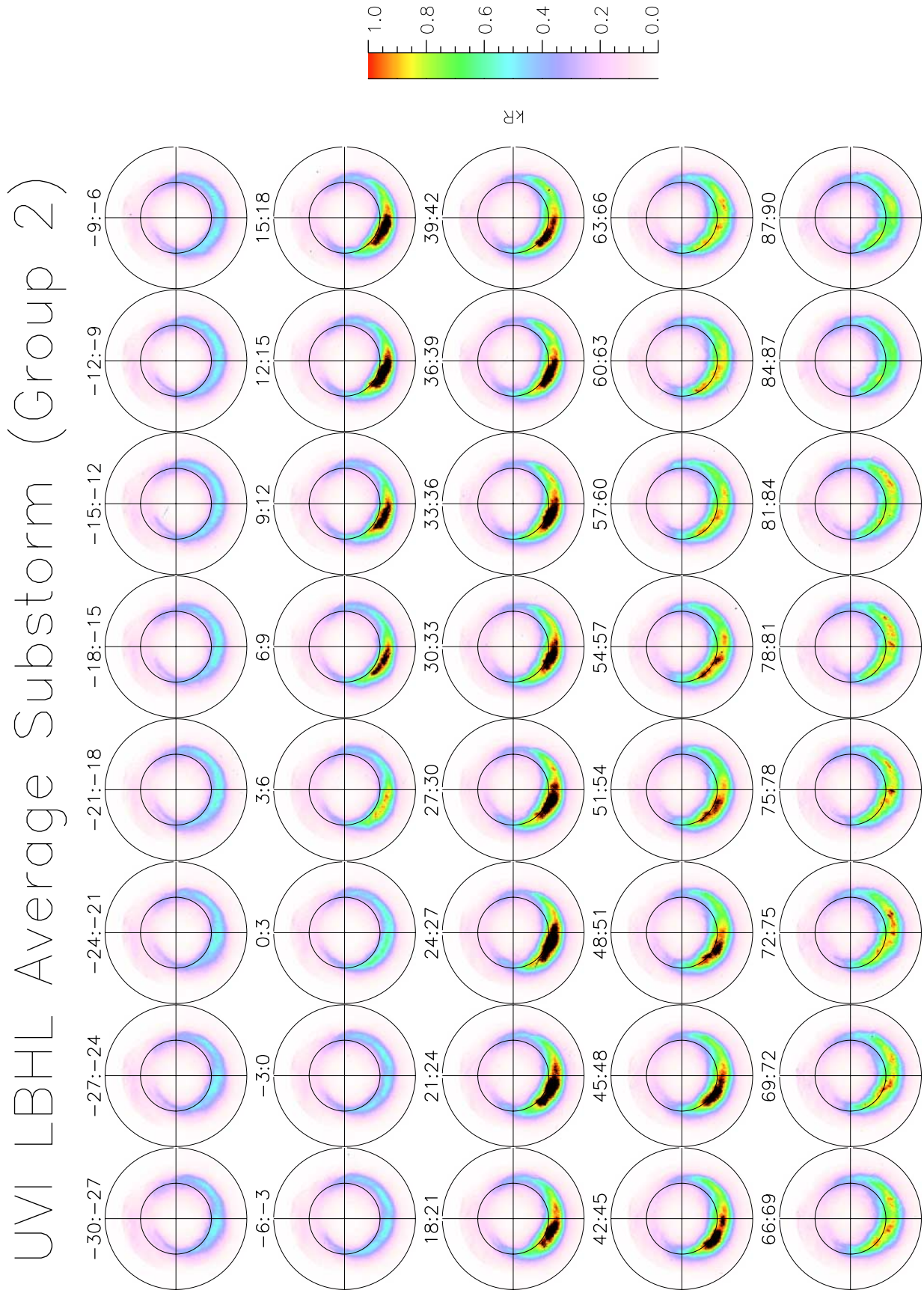

Figure 8. Images from 57 large substorms (group 2) were averaged together to produce this sequence of 40 composite images spanning the time interval from 30 min before onset to 90 min after. Format is the same as Figure 3.

Table 2. Average Ion Fluxes (cm^{-2} s^{-1})

	Group 1		Group 2		Group 1		Group 2	
Δt, min	Flux	Number	Flux	Number	Flux	Number	Flux	Number
	Nightside Auroral Zone O^+				*Nightside Auroral Zone H^+*			
−30–0	3.2×10^6	552	4.0×10^6	557	3.1×10^6	552	7.3×10^6	557
0–30	4.5×10^6	649	5.6×10^6	761	6.8×10^6	649	1.1×10^7	761
30–60	3.8×10^6	680	4.8×10^6	1163	8.7×10^6	680	5.6×10^6	1163
60–90	1.9×10^6	347	4.5×10^6	115	3.6×10^6	347	1.1×10^7	115
	Polar Cap O^+				*Polar Cap H^+*			
−30–0	4.3×10^5	417	6.7×10^5	560	1.4×10^5	417	4.1×10^5	560
0–30	2.9×10^5	657	2.4×10^5	571	4.4×10^5	657	2.8×10^5	571
30–60	5.6×10^5	596	1.8×10^5	275	5.8×10^5	596	5.5×10^4	275
60–90	4.7×10^5	228	2.9×10^5	124	3.5×10^5	228	5.6×10^5	124

shows these averages using 30 min time bins. Figure 9 shows the distribution of FAST/TEAMS data points in MLT/MLat space for each of these time intervals. In addition to the average fluxes, Table 2 gives the number of data points used for each average.

[31] The fluxes listed in Table 2 illustrate several points. First, the average fluxes in the nightside auroral zone tend to be higher for group 2 substorms compared to group 1 substorms. Second, there is a noticeable jump in the auroral zone average flux after onset. Third, the average fluxes in the nightside auroral zone are a factor of 4–40 times larger than the corresponding flux in the polar cap. Fourth, after onset there is a tendency for the average flux in the polar cap to drop; more for the larger substorms than the smaller substorms. Toward the end of the interval (60–90 min) there is an apparent recovery of polar cap averages but the small number of measurements in this last interval reduces confidence in this conclusion.

[32] With the area of each region and the average fluxes from Table 2 we can find the O^+ and H^+ ion outflow rates as a function of time. Rather than use the Table 2 fluxes we used a running box car average of the FAST/TEAMS data (30 min

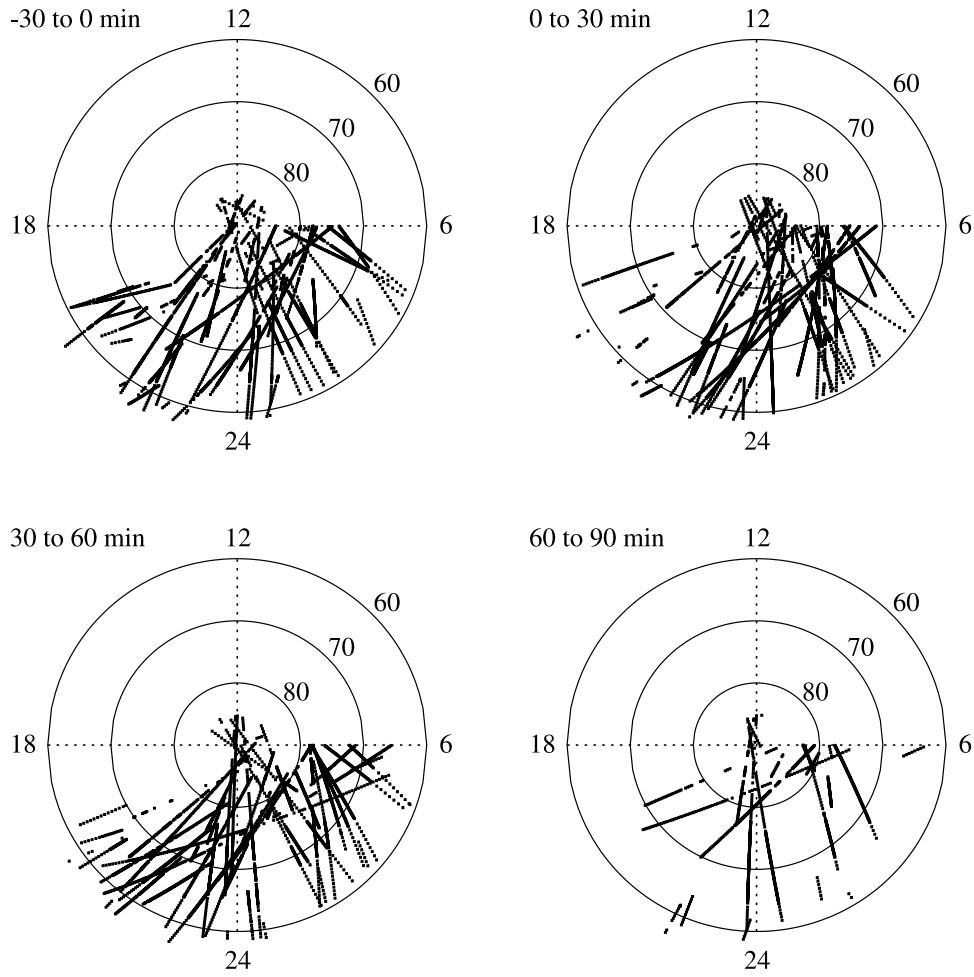

Figure 9. Distribution of FAST/TEAMS ion measurements in four 30 min time bins, starting 30 min before onset to 90 min after.

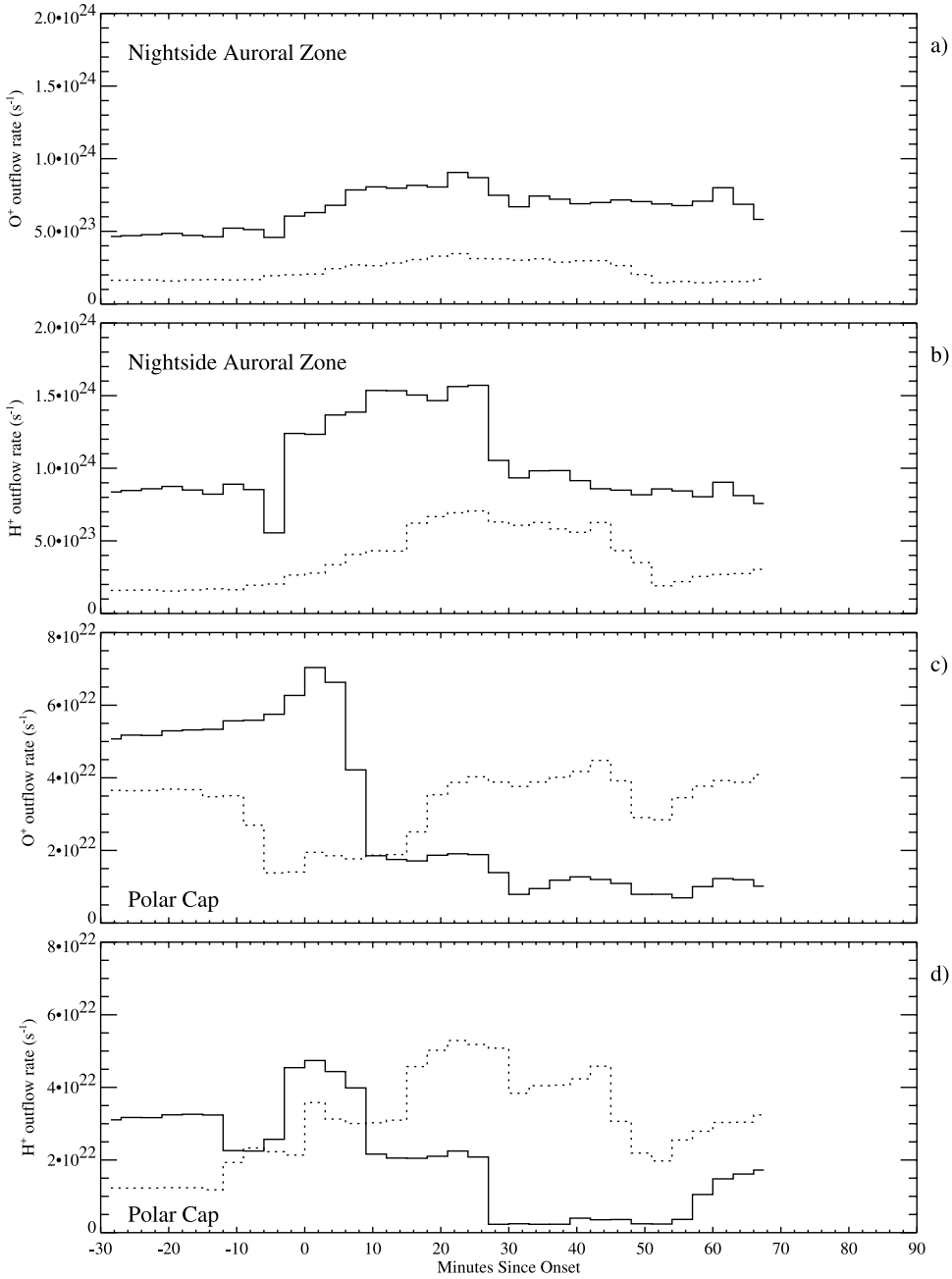

Figure 10. (a) Nightside auroral zone O^+ outflow rate as a function of time since onset. Solid line is for large substorms (group 2) and dotted line for small substorms (group 1). The nightside auroral zone is defined the same as in Figure 6. (b) Same as Figure 10a but for H^+ ions. (c) Polar cap O^+ ion outflow rate as a function of time since onset. The polar cap is defined the same as in Figure 6. (d) Same as Figure 10c but for H^+ ions.

window) to find the average flux as a function of time. The trend in these values follows the trends seen in Table 2. The ion outflow rates versus time are plotted in Figure 10. No points are plotted past about 70 min because of the lack of FAST data at the later times as is evident in Figure 9.

[33] In general the time variation of these regional ion outflow rates are very similar to what is seen in Figure 6. The levels are very similar. The large substorm group (2) has higher nightside auroral zone outflow rates than the small substorm group (1). There is about a factor of 2 increase in the ion outflow rate from the nightside auroral zone after onset for most cases except for H^+ from group 1 substorms where the increase is about a factor 3. The pre-onset polar cap outflow rates are about $3-5 \times 10^{22}$ ions/s for O^+ and $1-3 \times 10^{22}$ ions/s for H^+ for all types of substorms in Figures 6 and 10.

[34] The results in Figure 10 suggest that there is an increase in the polar cap outflow rate of both O^+ and H^+ during the growth phase for group 2 substorms followed by a large drop in these rates after onset. For group 1 substorms the O^+ polar cap outflow rate drops before onset and then increases after while the H^+ outflow rate increases after

Table 3. Size of Polar Cap and Nightside Auroral Zone (10^6 km^2)

	Polar Cap			Nightside Auroral Zone		
	−15–0 min	18–30 min	30–60 min	−15–0 min	18–30 min	30–60 min
Small	9.3	8.5	8.3	2.9	4.2	4.4
Medium	9.0	7.7	7.5	7.3	9.4	9.6
Large	7.7	6.2	5.6	14.7	18.1	18.1

onset. On the other hand, the results in Figure 6 suggest that the polar cap outflow rates for small and medium substorms should remain unchanged while for large substorms they would drop by about a factor of two by the time the recovery phase has begun. The Figure 6 results occur because the area and the average luminosity of the polar cap remain unchanged during all but the largest of these substorms. The Figure 10 results occur because some subsets of the low luminosity FAST data (e.g., compare group 2 H^+ polar cap to group 1 H^+ polar cap) have lower average fluxes than other parts. When the eight flux values from the polar cap H^+ portion of table 2 are averaged together one gets a value of 3.6×10^5 cm^{-2} s^{-1}; the same value obtained for H^+ in the polar cap in the previous method.

[35] Another difference between the Figures 6 and 10 results is the drop in group 2 O^+ and H^+ (larger for H^+) auroral zone outflow rates after about 30 min. The auroral zone outflow rate for large and medium substorms in Figure 6 does not show such a drop. Why the difference? These drops are not the result of a decrease in the area or total luminosity of the nightside auroral zone for group 2 substorms but reflect a drop in the average ion outflow flux about 30 min after onset. This is another point on which these two approaches differ.

4. Discussion

[36] To summarize the results, the following applies. The nightside auroral zone ion outflow rate increases with increasing substorm size. From the smallest to the largest storms seen in this data set this rate increases by about a factor of 10 for both O^+ and H^+ ions as Figure 6 illustrates. If we combine both the polar cap and the nightside auroral zone the outflow rate goes up by a factor of 7 for both H^+ and O^+ for the same change in conditions. When substorm onset occurs, the nightside auroral zone ion outflow rate increases by about a factor of two for each ion species regardless of substorm size. What these numbers tell us is that the nightside auroral zone can supply more ions to the plasma sheet prior to the onset of a large substorm then it would supply post onset for a small storm. For these wintertime solar minimum conditions the H^+ outflow rate is consistently about a factor of 2 larger then the O^+ outflow rate but only in the auroral zone. In the polar cap these rates are comparable. It should be emphasized that the time histories of ion outflow rates shown in Figures 6 and 10 only represent the gross features since short duration spikes would be washed out by the averaging we have had to apply here.

[37] The increase in nightside auroral zone ion outflow rate from a group 1 substorm to a group 2 substorm (from Figure 10) is a factor of 3.5 for H^+ and 2.7 for O^+. Adding the polar cap to the nightside auroral zone does not change these values by much. These increases are less than those found in the other method in large part because of the smaller difference in size between the group 1 and group 2 auroral zones when compared with the size difference between small and large substorms from the first method. Because of this we feel that the first method is superior since it has less of a tendency smooth out variations that likely exist in the real system.

[38] The question arises here as to how much of the change in ion outflow rates are due to changes in the average ion fluxes and how much is due to changes in the size of the polar cap or nightside auroral zone. Table 3 shows the size of the polar cap and nightside auroral zone averaged over different time intervals for small, medium and large (from Figures 3–5) substorms. From small to large substorms the nightside auroral zone increases in size by a factor of 4–5. This means that the average nightside auroral zone O^+ flux increases by a factor of about 2 for the same change so that most of the increase in this outflow rate is attributable to an increase in the size of the auroral zone. For large substorms most of the factor-of-2 increase in the nightside auroral zone outflow rate that occurs after onset is a result of an increase in the average ion flux. For small substorms the increase is about evenly divided between both effects. All of the change noted in the polar cap outflow rates in Figure 6 can be attributed to changes in the area of the polar cap.

[39] How do our outflow rates compare with previous estimates? *Yau et al.* [1998] combined several years of DE1/EICS data to derive expressions giving the total (auroral zone, cleft ion fountain, polar cap) ion outflow rate as a function of species, solar activity and magnetic activity. Table 4 lists results from these expressions assuming a value of $F_{10.7}$ of 73 and a Kp of 2+. *Collin et al.* [1989] reexamined the same data set and obtained a slightly different set of expressions (see *Peterson et al.* [2001] for the expressions) which give lower outflow rates for the same conditions. These values are also listed in Table 4. Finally, *Peterson et al.* [2001] used Polar/TIMAS perigee data to produce MLT-invariant latitude maps of H^+, O^+ and He^+ outflow for three southern winter (1996, 1997, 1998) and two southern summer (1997, 1998) seasons. The values listed in Table 4 are for southern winter 1996 (April to September 1996) when the average value of $F_{10.7}$ was 72. The average Kp for the Polar data set was 2-. The last column in Table 4 gives our average results, adding the polar cap outflows to the nightside auroral zone values, using values from medium substorm traces in Figure 6. These values were used for the average because we had more medium size substorms than any other size and because the average value of Kp during the medium substorms was the same as the average for the data set as a whole.

[40] The results of *Yau et al.* [1998] and *Collin et al.* [1989] indicate that as magnetic activity increases, the O^+ outflow rate should increase more rapidly than the H^+ outflow rate. The average Kp for our small storms is 1+

Table 4. Ion Outflow Rates (ions/s)

Ion	*Yau et al.* [1998]	*Collin et al.* [1989]	*Peterson et al.* [2001]	Current Work
H^+	2.4×10^{25}	1.7×10^{25}	3.8×10^{24}	6.3×10^{23}
O^+	1.2×10^{25}	7.6×10^{24}	3.0×10^{24}	3.3×10^{23}
H^+/O^+	2.0	2.2	1.3	1.9

and for our large storms is 4+. For this change of Kp these authors predict that the H^+ outflow rate should go up by a factor of 2 and the O^+ outflow rate should increase by a factor of 5. Our change in outflow rate for both the polar cap and nightside auroral zone increases by a factor of 7 for both H^+ and O^+ ions. The change in the O^+ rate is not too different from the previous value of 5 but the H^+ rate change is significantly different. Bear in mind here that we do not include any contributions to our outflow rates from the dayside auroral zone. This may very well account for the difference between our H^+ rate changes and those of *Yau et al.* [1998] and *Collin et al.* [1989].

[41] One should note from Table 4 that our outflow rates are lower than the other three estimates. This is likely due to several reasons. First we cover only the polar cap and the nightside auroral zone while the other estimates cover the entire high latitude region. This suggests that for these conditions the dayside auroral zone and cleft ion fountain supply 5 to 37 times as much H^+ and 8 to 35 times as much O^+ as the nightside auroral zone and polar cap do. Interestingly enough, the average *Peterson et al.* [2001] results (see Table 5 in their paper) indicate that 17% of the O^+ outflow comes from the nightside auroral zone and polar cap while 50% of the H^+ comes from that region. Another reason for the difference in rates is the energy range coverage of the different instruments used in these studies. The *Yau et al.* [1998] and the *Collin et al.* [1989] studies used data from the DE1/EICS instrument which sampled energies from 10 eV to 17 keV. The *Peterson et al.* [2001] data set extended from 15 eV to 33 keV. Our TEAMS data set goes from 8 eV to 6 keV.

[42] Another thing to note from Table 4 is that all of the estimates for ion outflow rates predict that under the given conditions the H^+ rate should be about two times the O^+ rate. Our value for this ratio is in line with these expectations and is very close to that from *Yau et al.* [1998].

[43] *Tung et al.* [2001], using IESA (Ion Electrostatic Analyzer) data from FAST, report the observation of intense ($\geq 10^8$ cm^{-2} s^{-1}) ion upflow conic events at the poleward boundary of the nightside auroral zone. They state that these events are correlated with active aurora, including substorm expansion phase. Using UVI auroral images they estimate the size of the region where this upflow occurs and then calculate a total outflow rate that falls between 10^{22} and 10^{24} ions/s. These upflow events represent a portion of the total nightside auroral zone outflow since the average MLT width of these regions was 2 hours. We note, from Figure 6 results, that the total, after onset, nightside auroral zone ion outflow rate ($H^+ + O^+$) for small, medium and large substorms is 3×10^{23}, 9×10^{23}, and 2.5×10^{24} ions/s, respectively.

[44] Figure 2 in *Daglis et al.* [1996] shows a near simultaneous increase in the energy density of 17–300 keV O^+, H^+, and He^{++} ions in the near earth plasma-sheet ($-8.8\ R_E \leq x \leq -8.0\ R_E$, with MLT between 2000 and 0400) at substorm onset. In order for O^+ and H^+ ions flowing out of the nightside auroral zone to contribute to this pressure they would have to experience energization from a few 100 eV to about 50 keV while in route to the plasma sheet. The fact that the AMPTE/CCE data indicate that the O^+ and H^+ 17–300 keV pressures increase simultaneous would argue that the O^+ ions should be heated very quickly so that there is no time-of-flight delays relative to H^+. Our results show that the O^+ and H^+ nightside auroral zone outflow rates increase by about a factor of 2 over a period of 15 to 20 min after onset. This is a slower rise time than that in Figure 2 in the work of *Daglis et al.* [1996] for the plasma sheet pressure increase. From these considerations and the fact that the pressure of the 1–17 keV ions shows very little change at onset, we conclude that most of the pressure increase seen at onset in the work of *Daglis et al.* [1996] is due to local energization and not to prompt ionospheric outflow. Such energization resulting from the electric fields generated by dipolarization has been predicted by particle calculations [*Delcourt et al.*, 1990; *Sánchez et al.*, 1993] and observed in Geotail data [*Nosé et al.*, 2000].

[45] Our results indicate that substorm onset can lead to an increase in the outflow rate from the nightside ionosphere but that increase is not as significant as what occurs as a result of the overall increase in activity that may precede the substorm onset.

Appendix A

Table A1. December 1996 Substorm List

Onset Date/Time	Size	Group	Kp	Dst	$F_{10.7}$
96/12/04 1136	M	1	1+	3	69
96/12/04 1919	M	1	3	−14	69
96/12/04 2141	M	2	3	−14	69
96/12/09 0900	M	1	0+	7	72
96/12/09 1254	S	1	1	11	72
96/12/10 0356	M	2	3	−32	70
96/12/10 0730	L	2	5−	−26	70
96/12/15 0259	M	1	3−	−6	82
96/12/15 2050	L	2	4−	−21	82
96/12/16 0459	L	2	2+	−8	84
96/12/17 1455	M	1	1+	−14	84
96/12/18 1918	M	1	1+	−13	86
96/12/21 0417	SM	1	2−	5	81
96/12/21 2151	M	1	2+	−14	81
96/12/22 0104	M	1	2−	−12	79
96/12/22 0911	M	1	1	−7	79
96/12/22 1249	ML	2	3−	−6	79
96/12/22 1630	ML	2	3−	−28	79
96/12/24 0314	SM	1	2−	−4	76
96/12/24 1850	S	1	1−	−6	76
96/12/25 0822	M	2	2	−9	75
96/12/25 1038	M	2	2−	−26	75
96/12/25 1452	M	1	2	−23	75
96/12/26 0935	S	1	1−	−8	73
96/12/27 0236	S	1	2	−6	72
96/12/27 1427	S	1	0+	1	72
96/12/28 0806	SM	1	1−	−6	72
96/12/28 1021	ML	2	2−	−16	72
96/12/28 1646	SM	1	1−	1	72
96/12/29 0549	S	1	0+	−1	71
96/12/29 1834	M	1	1+	−3	71
96/12/30 2122	M	2	2+	−13	70
96/12/31 0633	S	1	1	−8	70
96/12/31 1135	SM	1	1	−12	70

Table A2. January 1997 Substorm List

Onset Date/Time	Size	Group	Kp	Dst	$F_{10.7}$
97/01/02 1253	SM	1	2−	7	70
97/01/02 1614	M	1	2−	−5	70
97/01/02 1840	S	1	2−	−3	70
97/01/02 2021	S	1	2−	−8	70
97/01/03 0550	S	1	1−	3	71
97/01/03 2147	M	1	1	2	71
97/01/04 0140	SM	1	1+	−3	71
97/01/04 0455	M	1	1	−1	71
97/01/06 0241	M	1	1−	9	71
97/01/07 0055	M	1	2+	23	71
97/01/07 0302	L	2	4	−1	71
97/01/08 0918	SM	1	1	−11	71
97/01/08 1412	M	2	2	−4	71
97/01/09 1744	SM	1	0+	−1	71
97/01/11 0829	M	1	2+	−18	72
97/01/12 0724	L	2	5−	−20	72
97/01/12 1640	M	2	3−	−14	72
97/01/13 0121	S	1	2	−16	72
97/01/14 0626	M	1	1+	−16	72
97/01/14 1152	M	1	1−	−17	72
97/01/15 0820	SM	1	1	−7	73
97/01/15 1520	M	1	2	−2	73
97/01/16 0846	SM	1	1−	−14	72
97/01/17 1857	SM	1	1	3	72
97/01/17 2130	SM	1	1+	1	72
97/01/18 1944	M	1	1−	1	72
97/01/19 0942	SM	1	1	−5	73
97/01/19 1546	ML	2	3	−19	73
97/01/21 0208	M	2	3+	−25	72
97/01/21 1200	M	2	2	−17	72
97/01/22 0508	M	2	2+	−10	71
97/01/22 1544	M	1	2−	−14	71
97/01/24 1300	SM	1	1−	−1	72
97/01/24 1642	S	1	1+	1	72
97/01/25 1245	M	1	1	−11	71
97/01/25 2014	ML	2	2+	−5	71
97/01/26 0216	M	1	2+	11	72
97/01/26 1614	ML	2	4−	−21	72
97/01/26 1818	L	2	4+	−32	72
97/01/27 1014	L	2	3−	−21	71
97/01/27 1601	M	2	3+	−11	71
97/01/27 1854	ML	2	3+	−22	71
97/01/28 1001	SM	1	3−	−32	71
97/01/28 1159	L	2	3−	−30	71
97/01/29 0523	M	1	2	−22	72
97/01/29 1406	M	2	2	−26	72
97/01/30 0840	SM	1	3−	−18	72
97/01/30 1130	SM	1	1+	−18	72
97/01/30 1646	ML	2	4	−18	72
97/01/31 0201	ML	2	3−	−16	70
97/01/31 1728	M	1	2−	−15	70
97/01/31 2015	M	2	2	−16	70

Table A3. February 1997 Substorm List

Onset Date/Time	Size	Group	Kp	Dst	$F_{10.7}$
97/02/01 1345	M	2	2+	−14	69
97/02/02 1606	ML	2	3+	−15	76
97/02/03 0332	S	1	1	−20	77
97/02/03 2116	SM	1	3−	−15	77
97/02/04 1054	M	1	2	−7	78
97/02/04 1334	M	2	1+	−14	78
97/02/06 0428	ML	2	4−	−10	72
97/02/06 0737	ML	2	3+	−16	72
97/02/08 1147	ML	2	3−	−5	73
97/02/09 0059	M	2	2+	−18	71
97/02/09 1407	L	2	3+	−13	71
97/02/09 1947	L	2	5+	−54	71
97/02/09 2125	L	2	4	−56	71
97/02/11 0041	ML	2	3	−45	69
97/02/11 0732	L	2	4	−40	69
97/02/11 1943	L	2	3+	−37	69
97/02/11 2222	ML	2	4+	−31	69
97/02/13 0534	SM	1	1+	−16	69
97/02/13 1147	M	1	1−	−12	69
97/02/14 0044	M	2	2−	−13	70
97/02/15 1352	SM	1	2−	−10	70
97/02/15 1553	M	2	3−	−23	70
97/02/17 0721	L	2	4+	−51	71
97/02/17 1956	M	2	2+	−26	71
97/02/18 1118	M	2	1+	−24	71
97/02/20 0101	S	1	1	−7	71
97/02/20 0347	S	1	2−	−7	71
97/02/20 0748	S	1	1	−2	71
97/02/21 1358	ML	2	3−	−23	72
97/02/21 1601	M	1	2	−13	72
97/02/22 0209	M	1	3−	−16	72
97/02/22 2158	ML	2	3−	−27	72
97/02/23 1431	S	1	2+	−1	73
97/02/25 0941	SM	1	1	−17	73
97/02/25 1856	M	2	1	−17	73
97/02/26 0211	M	2	3	−14	72
97/02/26 1219	ML	2	4	−25	72
97/02/27 1132	S	1	1+	−26	72
97/02/27 1412	M	2	3+	−25	72
97/02/28 0052	L	2	5+	−76	72
97/02/28 0448	L	2	6+	−63	72

[47] **Acknowledgments.** Lou-Chuang Lee thanks Masahito Nosé and another reviewer for their assistance in evaluating this paper.

References

André, M., and A. Yau (1997), Theories and observations of ion energization and outflow in the high latitude magnetosphere, *Space Sci. Rev.*, *80*, 27.

Collin, H. L., W. K. Peterson, A. W. Yau, and E. G. Shelley (1989), An empirical model of ionospheric ion outflow as a function of solar EUV and magnetospheric activity, paper presented at IAGA Meeting, Int. Assoc. of Geomagn. and Aeron., Exeter, U.K.

Daglis, I. A., and W. I. Axford (1996), Fast ionospheric response to enhanced activity in geospace: Ion feeding of the inner magnetotail, *J. Geophys. Res.*, *101*, 5047.

Delcourt, D. C., J. A. Sauvaud, and A. Pedersen (1990), Dynamics of single-particle orbits during substorm expansion phase, *J. Geophys. Res.*, *95*, 20,853.

Kozyra, J. U., M. W. Liemohn, C. R. Clauer, A. J. Ridley, M. F. Thomsen, J. E. Borovsky, J. L. Roeder, V. K. Jordanova, and W. D. Gonzalez (2002), Multistep *Dst* development and ring current composition changes during the 4–6 June 1991 magnetic storm, *J. Geophys. Res.*, *107*(A8), 1224, doi:10.1029/2001JA000023.

Liou, K., P. T. Newell, D. G. Sibeck, C.-I. Meng, M. Brittnacher, and G. Parks (2001), Observations of IMF and seasonal effects in the location of auroral substorm onset, *J. Geophys. Res.*, *106*, 5799.

Möbius, E., et al. (1998), The 3D plasma distribution function analyzers with time-of-flight mass discrimination for Cluster, FAST, and Equator-S, in *Measurement Techniques in Space Plasmas*: *Particles*, *Geophys. Monogr. Ser.*, vol. 102, edited by R. F. Pfaff, J. E. Borovsky, and D. T. Young, p. 243, AGU, Washington, D.C.

Moore, T. E., and D. C. Delcourt (1995), The geopause, *Rev. Geophys.*, *33*, 175.

Norqvist, P., M. André, and M. Tyrland (1998), A statistical study of ion energization mechanisms in the auroral region, *J. Geophys. Res.*, *103*, 23,459.

Nosé, M. A., T. Y. Lui, S. Ohtani, B. H. Mauk, R. W. McEntire, D. J. Williams, T. Mukai, and K. Yumoto (2000), Acceleration of oxygen ions of ionospheric origin in the near-Earth magnetotail during substorms, *J. Geophys. Res.*, *105*, 7669.

Øieroset, M., M. Yamauchi, L. Liszka, S. P. Christon, and B. Hultqvist (1999), A statistical study of ion beams and conics from the dayside ionosphere during different phases of a substorm, *J. Geophys. Res.*, *104*, 6987.

Peterson, W. K., H. L. Collin, A. W. Yau, and O. W. Lennartsson (2001), Polar/toroidal imaging mass-angle spectrograph observations of suprathermal ion outflow during solar minimum conditions, *J. Geophys. Res.*, *106*, 6059.

Sánchez, E. R., B. H. Mauk, and C.-I. Meng (1993), Adiabatic vs. non-adiabatic particle distributions during convection surges, *Geophys. Res. Lett.*, *20*, 177.

Stevenson, B. A., J. L. Horwitz, G. Germany, T. E. Moore, B. L. Giles, P. D. Craven, M. O. Chandler, Y.-J. Su, and G. K. Parks (2001), Polar observations of topside field-aligned O^+ flows and auroral forms, *J. Geophys. Res.*, *106*, 18,969.

Torr, M. R., et al. (1995), A far ultraviolet imager for the international solar-terrestrial physics mission, in *The Global Geospace Mission*, edited by C. T. Russell, p. 329, Kluwer Acad., Norwell, Mass.

Tung, Y.-K., C. W. Carlson, J. P. McFadden, D. M. Klumpar, G. K. Parks, W. J. Peria, and K. Liou (2001), Auroral polar cap boundary ion conic outflow observed on FAST, *J. Geophys. Res.*, *106*, 3603.

Wilson, G. R., D. M. Ober, G. A. Germany, and E. J. Lund (2001), The relationship between suprathermal heavy ion outflow and auroral electron energy deposition: Polar/Ultra-violet Imager and Fast Auroral Snapshot/Time-of-Flight Energy Angle Mass Spectro-meter observations, *J. Geophys. Res.*, *106*, 18,981.

Winglee, R. M. (1998), Multi-fluid simulations of the magnetosphere: The identification of the geopause and its variation with IMF, *Geophys. Res. Lett.*, *25*, 4441.

Yau, A., and M. André (1997), Source of ion outflow in the high latitude ionosphere, *Space Sci. Rev.*, *80*, 1.

Yau, A. W., P. H. Beckwith, W. K. Peterson, and E. G. Shelley (1985), Long-term (solar cycle) and seasonal variations of upflowing ionospheric ion events at DE1 altitudes, *J. Geophys. Res.*, *90*, 6395.

Yau, A. W., W. K. Peterson, and E. G. Shelley (1998), Quantitative parameterization of energetic ionospheric ion outflow, in *Modeling Magnetospheric Plasma*, *Geophys. Monogr. Ser.*, vol. 44, edited by T. E. Moore and J. H. Waite Jr., p. 211, AGU, Washington, D.C.

Young, D. T., H. Balsiger, and J. Geiss (1982), Correlations of magnetospheric ion composition with geomagnetic and solar activity, *J. Geophys. Res.*, *87*, 9077.

G. A. Germany, Center for Space Plasma and Aeronomic Research, University of Alabama in Huntsville, S131 Technology Hall, Huntsville, AL 35899, USA. (germanyg@cspar.uah.edu)

E. J. Lund, Space Science Center, University of New Hampshire, Morse Hall, 39 College Road, Durham, NH 03824, USA. (lund@atlas.sr.unh.edu)

D. M. Ober and G. R. Wilson, Mission Research Corporation, 589 Hollis Street, Suite 201, Nashua, NH 03062, USA. (dober@mrcnh.com; gwilson@mrcnh.com)